Rapid and delayed effects of single-walled carbon nanotubes in glioma cells

Lena Golubewa [1,2], Tatsiana Kulahava [2], Igor Timoshchenko [2,3], Mikhail Shuba [2],

Yuri Svirko [4], Polina Kuzhir [2,4,∗]

[1]*Department of Molecular Compounds Physics, State research institute Center for Physical*

Sciences and Technology, Saulėtekio av. 3, Vilnius, 10257, Lithuania. E-mail:

lena.golubewa@ftmc.lt

[2]*Laboratory of Nanoelectromagnetics, Institute for Nuclear Problems of Belarusian State*

University, Bobruiskaya str. 11, Minsk, 220006, Belarus

[3]*Department of Computer Modelling, Physics Faculty, Belarusian State University,*

Bobruiskaya str. 5, Minsk, 220030, Belarus

[4]*Institute of Photonics, Department of Physics and Mathematics, University of Eastern*

Finland, Yliopistokatu 7, Joensuu, 80101, Finland

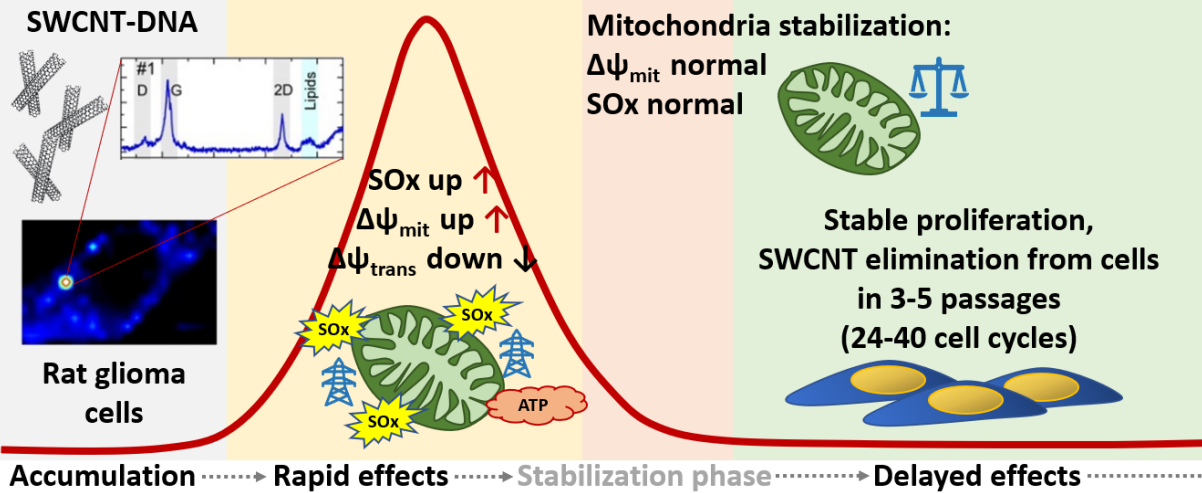*Corresponding author: Tel: +358505666624. E-mail: polina.kuzhir@uef.fi

Abstract

Single-walled carbon nanotubes (SWCNTs) demonstrate a strong potential as an optically activated theranostic nano-agent. However, using SWCNTs in theranostics still requires revealing mechanisms of the SWCNT-mediated effects on cellular functions. Even though rapid and delayed cellular responses can differ significantly and may lead to undesirable consequences, understanding of these mechanisms is still incomplete. We demonstrate that introducing short (150–250 nm) SWCNTs into C6 rat glioma cells leads to SWCNT-driven effects that show pronounced time dependence. Accumulation of SWCNTs is carried out due to endocytosis with modification of the actin cytoskeleton but not accompanied with autophagy.

1

Its initial stage launches a rapid cellular response via significantly heightened mitochondrial membrane potential and superoxide anion radical production, satisfying the cell demand of energy for SWCNT transfer inside the cytoplasm. In the long term, SWCNTs agglomerate to micron-sized structures surrounded by highly active mitochondria having parameters return to control values. SWCNTs postponed effects are also manifested themselves in the suppression of the cell proliferative activity with further restoration after five passages. These results demonstrate relative cellular inertness and safety of SWCNTs eliminating possible side effects caused by optically activated theranostic applications.

Keywords: single-walled carbon nanotubes, endocytosis, autophagy, mitochondrial membrane potential, superoxide, theranostics

Graphical abstract

SWCNT-DNA

Rat glioma cells

SOx up ↑
Δψ$_{mit}$ up ↑
Δψ$_{trans}$ down ↓

Mitochondria stabilization:
Δψ$_{mit}$ normal
SOx normal

Stable proliferation,
SWCNT elimination from cells
in 3-5 passages
(24-40 cell cycles)

Accumulation ·······▸ Rapid effects ·······▸ Stabilization phase ···········▸ Delayed effects ···············

1. Introduction

In cancer treatment, visualization of a tumor or tracking drug delivery to the tumor site can be performed by an agent having therapeutic potential. Such an approach is often referred to as theranostics, i.e., a combination of the diagnosis and therapeutic techniques, while the agents capable of combining diagnostics and treatment are referred to as theranostic agents. They can be either medicinal compounds themselves, or nano-entities capable of acquiring specific physicochemical properties under the external influence [1], such as irradiation with near-infrared (NIR) photons [2] or neutrons [3]. There is growing evidence that inorganic nanomaterials ought to be biodegradable, clearable and possess no long-term cytotoxicity [XX]; thus, a significant attempt should be made towards the safe design of inorganic theranostic nanoagents [XXX].

Single-walled (SW) and multi-walled (MW) carbon nanotubes (CNTs) exhibit unique physical, chemical, and biological properties [4], [5], [6], which allow one to use them in a capacity of theranostic agents. Nano-needle shape with a hollow core and high aspect ratio [7] makes it possible to use SWCNTs and MWCNTs for drug delivery, well-developed functionalization allows one to employ them to target the tumor [8], while their intense Raman spectra can be employed to visualize tumor cells [9]. That is, CNTs are capable to provide (i) a source of imaging signal, (ii) a therapeutic drug, (iii) a carrier of a therapeutic drug, and (iv) targeting ligand for selective accumulation in the tumor [10].

Nevertheless, several problems preventing using CNTs and/or suppressing their efficiency in theranostics still remain unresolved. The most important one is the strong van der Waals attraction between CNTs dispersed in water that results in the formation of aggregates and agglomerates [11], which may lead to undesirable effects including immune cell activation (inflammation) [12], [13] and platelet activation (thrombosis) [14]. The theranostic applications require uniform aquatic CNTs suspensions having suppressed aggregation level in a broad concentration range, stability with respect to the sedimentation, and biocompatibility [15]. In

4

this regard, additional functionalization with edge functional groups or complexes with macromolecules (DNA, nucleotides, etc.) turns out to be necessary. CNT penetration throughout the cell plasma membrane and their stable accumulation during CNT-based drugs administration should be determined in such a way as to regulate accumulation time, intracellular CNTs concentration and distribution. CNT length may also influence the efficiency of therapeutic applications of CNTs. Commonly used SWCNTs are of a micron-sized length (up to 20 μm) and exhibit pronounced length-dependent cytotoxicity [XXXX], thus accurate control of SWCNT size distribution and fabrication of short-length SWCNTs are necessary for improving the efficiency. Moreover, SWCNTs, MWCNTs and other graphene derivatives such as graphene and graphene oxide (GO) sheets, quantum dots due to the presence of functional groups at the edges and/or in planes of graphene, could induce oxidative stress due to the involvement of edge/in-plane groups in redox processes [1, 2]. Different spatial-volumetric characteristics and surface functional groups on graphene derivatives determine the efficiency of nanomaterial complexation with biomolecules and the properties of obtained complexes [4]. This might influence the accumulation mechanism of CNTs, GO/graphene sheets, etc., and determine the effects of complexes on cell functional activity as well. In addition, essential factors in any anticancer therapy are the side effects that agents can have besides their primary therapeutic function. In this regard, the question about delayed effects produced by agents that were not involved in therapy for any reason and not undergone destruction remains unclear.

We have recently demonstrated the destruction of CNT-accumulated glioma cells under irradiation with NIR laser pulses [16]. The developed model has shown that depending on the parameters of SWCNTs and their agglomeration degree, one can achieve not only photothermal but also a "cold" photothermoacoustic destruction of tumor cells [16]. The latter regime allows one to suppress side effects, including tissue overheating and non-specific cell damage, while its efficiency is determined mainly by the concentration of the SWCNT agglomerates rather

than on where the cell accumulates SWCNTs. These findings confirm the paramount importance of revealing the mechanisms of SWCNT accumulation and intracellular aggregation.

In this paper, we visualize the distribution and localization of short-length (100-300 nm) SWCNTs, for better dispersibility covered with DNA (SWCNT-DNA), in C6 rat glioma cells using the confocal Raman microscopy. The obtained results confirm the micropinocytosis mechanism of SWCNT-DNA accumulation. The revealed immediate and delayed effects of SWCNTs on the cell mitochondrial function and proliferative activity open a way towards enhancement of the therapeutic efficacy and safety and develop personalized therapy.

2. Materials and methods

2.1 *Cell culture*

ATCC C6 (ATCC® CCL-107™) rat glioma cells were obtained from ATCC, LGC Standards, Ogrodowa 27/29, Kielpin, Poland. Cells were cultured in Petri dishes on the surface of silicon plates in DMEM medium (Gibco, USA) supplemented with 10% fetal bovine serum (FBS, Sigma Chemical Co., St. Louis, MO, USA), 8×10^{-4} g / mL of gentamicin sulfate (Belmedpreparaty, Belarus), and 2×10^{-3} M of glutamine (Sigma-Aldrich, USA) at 37 ºC in an atmosphere of 5% CO_2. The number of cells during subculturing was 0.5×10^5 cells per mL. The cells were allowed to adhere to the surface. DNA or SWCNT-DNA complexes were added with the culture medium to the cells after 6 h of the reseeding.

2.2 *Preparation of solutions of single-walled carbon nanotubes*

SWCNTs (Nanointegris Technology Inc., Batch PO568) produced by gas-phase catalysis (HiPCO process), in bundles, with purity exceeding 98% were used. Short (100-300 nm) SWCNTs were obtained by the method [17]. 0.5 mg of SWCNT material was placed in a mixture of acids (0.6 mL of nitric (65%) + 3 mL of sulfuric (95%)). The mixture was dispersed with an UZDN-2T ultrasonic disperser for 30 h at maximum power, ultrasonic frequency 44 kHz, at the lowest possible temperature of 4-8 °C. As a result, the length of the tubes was

significantly shortened and became less than 400 nm. To get rid of the acid, the tubes were diluted with water 1 to 20, centrifuged for 5 min at 900 g to precipitate, the non-precipitated part was discarded, and water was added to the settled part. This operation was performed 6 times to achieve a neutral environment. The tubes were stored in water as agglomerates.

The SWCNT suspension was added to an aqueous solution of DNA (Sigma Aldrich, USA) (or oligonucleotides (Primetech, Belarus)), pre-dispersed by ultrasound for 30 minutes (2 mg of DNA per 6 mL of DMEM) until a concentration of 100-200 μg / mL was reached, and then the mixture was dispersed by ultrasound for 2-4 hours at room temperature, centrifuged at 8000g for 15 minutes. Short SWCNTs (100-300 nm) were obtained with an average length of about 250 nm. Characterization of SWCNTs was performed by atomic force microscopy (AFM) and Raman spectroscopy (see Supporting Information, Fig. S1 and S2). Complexation of SWCNTs with DNA molecules led to the significant increase of solubility of SWCNTs and suspension stability (see Supporting Information, Fig. S3).

2.3 *Raman microscopy of the accumulation and distribution of complexes of carbon nanotubes in cells*

The distribution of SWCNTs in C6 rat glioma cells was studied by confocal Raman spectroscopy using a confocal Raman 3D scanning (fluorescence) microscope NanoFinder HighEnd (Tokyo Instruments, Tokyo, Japan - LotisTII, Minsk, Belarus). The distribution of SWCNTs was determined after 1–72 h of incubation of cells with SWCNTs at 37 ° C.

Cells were visualized using two lasers: 532 nm (20 mW) and 785 nm (75 mW). Exposure time was 1-10 s, scanning step - 1.5-2.0 microns according to the experimental series. To avoid cell damage, neutral density filters were used to reduce the intensity of laser radiation (for a 532 nm laser, the output power was 600 μW).

2.4 *Cell proliferation rate*

Before each experiment (3.5h, 7.5h, 21h and 24h) cells in every experimental set were washed with PBS (w/o FBS, $C2^{2+}$, Mg^{2+} ions), trypsinized, centrifuged for 3 min at 600g, media was

replaced by Hepes-buffer (NaCl – 131 mM, KCl – 5 mM, MgSO$_4$ – 1.3 mM, CaCl$_2$ – 1.3 mM, Hepes – 20 mM, C$_6$H$_{12}$O$_6$ – 5 mM), cells were resuspended and calculated using Goriaev Chamber.

2.5 *Autophagocytosis detection with monodancylcadaverine (MDC)*

After 48h in one experimental set, media containing FBS was replaced by DMEM w/o FBS to induce starvation-caused autophagocytosis (negative control). DNA or SWCNTs were added in equal aliquots so that the final concentration of SWCNTs was 5 μg/mL. Cells were exposed to SWCNT-DNA complexes or to DNA for 3.5h, 7.5h, 21h and 24h. Control cells were held with the NaCl water solution (0.15 M) of the same volume as DNA or SWCNT-DNA for the same time intervals.

After counting, cells were incubated with MDC (Merck, Germany) at a final concentration of 10 μM for 30 min in the dark. Then cells were centrifuged at 600g for 3 min twice. Cells were mounted in Hepes-buffer for all experiments. MDC fluorescence was detected using LSF 1211A spectrofluorometer (Solar, Belarus) with λ_{ex} = 335 nm in the range of 500÷600 nm. Results were performed as an integrated area under the MDC fluorescence emission spectra in the full range of wavelengths.

2.6 *Laser-scanning fluorescence microscopy of the actin cytoskeleton of glioma cells*

Cells were incubated for 1, 2, 18, and 24 h at 37 ° C in the presence of SWCNT-DNA, then fixed on glass substrates with 4% paraformaldehyde solution for 10 min at room temperature. The coverslips with the cell monolayer were washed three times with PBS, cell membranes were permeabilized with 0.1% Triton X-100 solution (Sigma-Aldrich, USA), washed three times with PBS, and 50 μL of CytoPainter Phalloidin-iFluor 532 (Abcam, UK) were added. The cell monolayer was incubated for 60 min at room temperature and 100% humidity. Then the coverslips were washed twice in PBS and once in distilled water fixed with glycerol on a slide. Measurements were performed on a confocal Raman 3D scanning (fluorescence) microscope NanoFinder HighEnd.

2.7 Mitochondrial membrane potential and superoxide anion-radicals production in cells under the action of SWCNT-DNA complexes

Mitochondrial membrane potential in glioma cells was studied by fluorescence analysis using a JC-1 fluorescent probe (Invitrogen, USA) and MitoSOX Red mitochondrial superoxide indicator (Invitrogen, USA) on a confocal Raman 3D scanning (fluorescence) microscope NanoFinderHighEnd and an LSF 1211A spectrofluorometer.

C6 rat glioma cells were incubated for 1, 2, 18, and 24 h with SWCNT-DNA at a concentration of 4.5 µg/mL. The cells were stained with JC-1 (7.5×10^{-7} M) for 15 min at 37 °C. The cells were washed twice in PBS. JC-1 fluorescence excitation was performed at $\lambda_{ex} = 473$ nm. The potential on the mitochondrial membrane was estimated from the ratio of the fluorescence intensities of the probe at $\lambda_{fl590} = 590$ nm (J-aggregates) and $\lambda_{fl530} = 530$ nm (monomeric form). The generation of superoxide radical anions by mitochondria was studied using MitoSOX Red. Cells were stained with MitoSOx Red (1.25×10^{-6} mol / L) for 20 min at 37 °C. Then the cells were washed twice in PBS. MitoSOx Red fluorescence was recorded using $\lambda_{ex} = 510$ nm and $\lambda_{em} = 580$ nm. Data are presented as integrated fluorescence intensity estimated over 10 min.

2.8 *Statistical processing of data*

The results were expressed as the means of three to five replicates ± SD. Statistical analysis was performed using the analysis of variance (ANOVA) with Bonferroni multiple comparison test for multiple pairwise comparisons with the respective control group. $p < 0.05$ was considered to be statistically significant. Data were presented using the OriginPro 8.0 software packages (OriginLab Corp., USA) and Microsoft Excel 2007 statistical software packages.

3. Results and Discussion

3.1 *Determination of the SWCNT-DNA non-toxic concentration*

Before studying the accumulation of SWCNT-DNA complexes in glioma cells, we investigated how the presence of the SWCNT-DNA complexes affected the number of viable cells in culture and revealed at which concentration SWCNTs are not toxic for normal cell division. We found that when the concentration of SWCNT-DNA exceeding 5 μg/mL, the number of viable cells was more than 10% lower than that observed compared to control cells without SWCNT-DNA complexes (see Figure 1a). SWCNT-DNA complexes at concentrations of 1.5-3.0 μg/mL lead to an increase in the number of cells compared to the control. The mechanism of this phenomenon is still unclear; however, it is out of the scope of this paper. Nevertheless, to avoid the undesirable influence of this phenomenon on the research results, in our experiment, we studied SWCNT-DNA complexes at the concentration of 5 μg/mL.
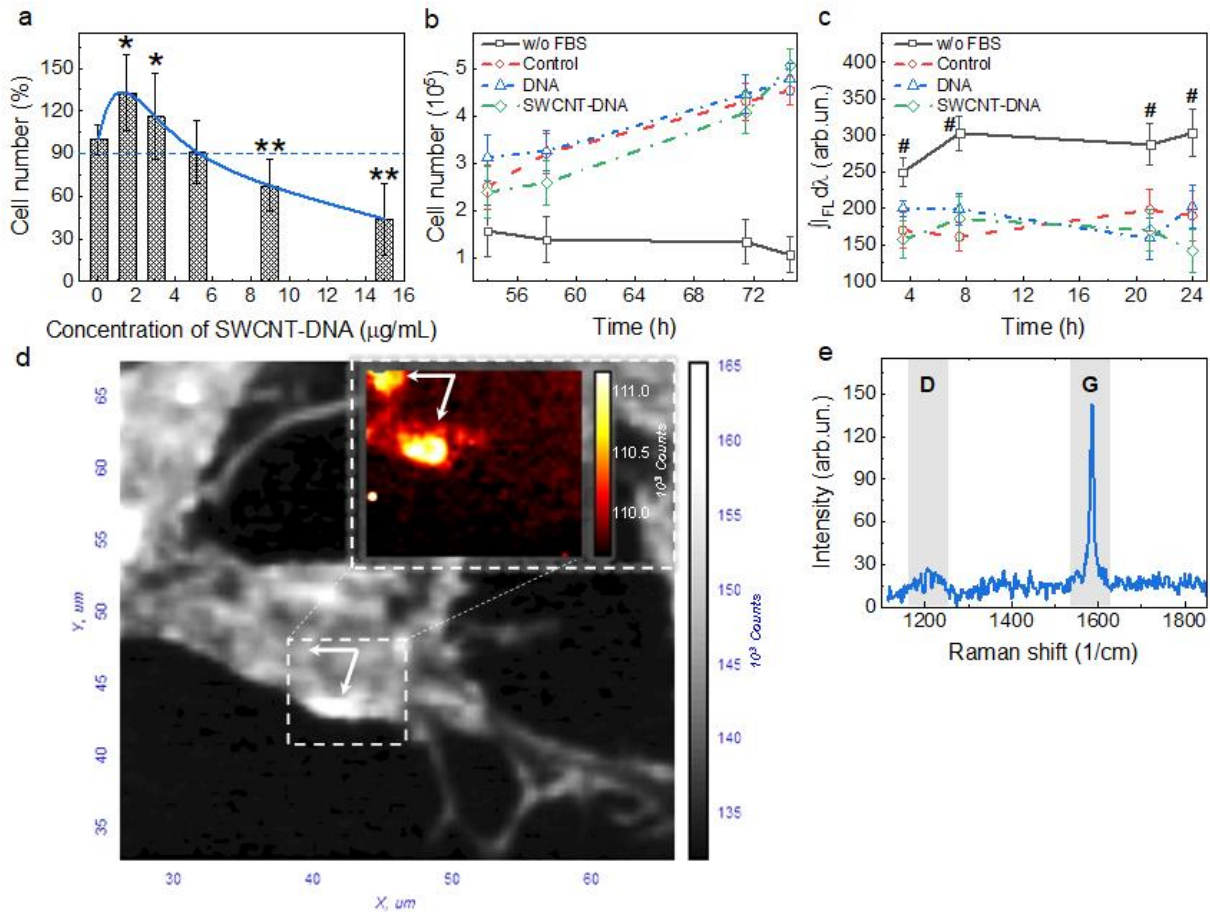
3.2 *Accumulation dynamics of SWCNT-DNA complexes inside C6 glioma cells*

Knowledge of the kinetics of the intracell SWCNTs accumulation is crucial for theranostics. SWCNTs are accumulated in macrophages, highly specialized phagocytic cells, in a non-monotonous manner via endocytosis. The accumulation rate is length-dependent with fast elimination of SWCNTs in 8 h via exocytosis [18]. We have already shown [9],[19] that in a non-phagocytic glioma cells, SWCNT accumulation lasts for more extended periods (>18 h), reaching saturation. In the present study, cells exposed to 5 μg/mL of SWCNT-DNA complexes, cells exposed to the DNA, and cells in control culture medium showed the same proliferation rate over 75 h, as presented in Figure 1b.

Interaction of CNTs with living cells and their accumulation inside has been widely discussed in terms of initiating autophagic cell death [20],[21], accompanied by an inflammatory response and oxidative stress [22]. Autophagy is a catabolic process of degradation and recycling of damaged organelles, debris, pathogens in specific double-membrane vacuoles in cells [23]. Fetal bovine serum (FBS) starvation was used as a negative

10

control model of induction of autophagic cell death [24]. In the starvation model, the number of cells after 26 h of growth in FBS-deficient media predictably decreased, being lower than the initially seeded ones. For autophagy detection, cell stained with fluorescent lysosomotropic probe monodansylcadaverine (MDC) was used. Preferential labelling of autophagic vacuoles with MDC via its interaction with lipids of the autophagosomes leads to its fluorescence increase [25]. That is, we demonstrate that SWCNT-DNA complexes at the concentration of 5 μg/mL do not exhibit significant cytotoxicity and mediate neither autophagy nor any acidic lysosome formation. The level of MDC fluorescence in cells exposed to SWCNT-DNA complexes, exposed to DNA, or in control cells is two times lower than that in starving cells with induced autophagy over the whole-time interval of observation (Figure 1c).

In ref [19] we have shown that interaction of SWCNT-DNA complexes with the C6 rat glioma cell membrane leads to the plasma membrane potential decrease, bending of the membrane inward, and formation of spherical structures near the membrane, allowing us to expect the energy-dependent endocytosis of SWCNT-DNA complexes. Simultaneous scanning confocal fluorescence and confocal Raman microscopy measurements reveal the transport vesicle-like structure formed around the SWCNT-DNA agglomerate. One can observe from Figure 1d that the formation of SWCNT-DNA agglomerates inside cells is accompanied by the fibrillar actin condensation (marked with a dashed square) around the agglomerate (see inset to Figure 1d and the Raman spectrum shown in Figure 1e). We expect that the F-actin cover of the agglomerate is formed around the transport vesicle to facilitate the transfer of the SWCNT agglomerate into the cell cytoplasm.

Figure 1. Cytotoxicity and accumulation dynamics of SWCNT-DNA complexes in C6 rat glioma cells. a – the number of viable cells exposed to SWCNT-DNA complexes at different concentrations. Cell viability was assessed using trypan blue stain as an exclusion test. Cell number was normalized to the control sample without SWCNT-DNA complexes and expressed in %. The dash-dot curve represents the data interpolation curve. The horizontal dash line defines 90% viability level. b – glioma cell survival over several cell cycles in control (with equivalent 0.15 M NaCl volume), in starvation cell model (FBS excluded from medium), in the presence of 30 μg/mL DNA or 5 μg/mL SWCNT-DNA complexes. c – autophagy determination in control (with equivalent 0.15 M NaCl volume), in starvation cell model (FBS excluded from medium), in the presence of 30 μg/mL DNA or 5 μg/mL SWCNT-DNA complexes; the intensity of autophagy process evaluated as the integrated intensity of MDC fluorescence spectra in the spectral range 500-600 nm. d – fluorescence image of F-actin cytoskeleton, stained with CytoPainter Phalloidin-iFluor 532 (λ_{ex} = 532 nm) in glioma cells exposed to SWCNT-DNA complexes for 18 h; inset – image of SWCNT-DNA agglomerate in cells obtained by Raman microscopy (λ_{ex} = 785 nm, P = 70 mW, step 0.8 μm). e – Raman spectrum of SWCNT, marked with the arrow in d. The lines connecting the points on the graphs are shown only to show the trend but do not carry much physical meaning. In a, b, c, data are mean ± SD values of duplicates from three independent experiments. *p < 0.05, **p < 0.01 refer to control without SWCNTs. #p < 0.01 refers to control and SWCNT-DNA.

Figure 2 summarizes data on the time-dependent accumulation of SWCNT-DNA complexes

over several cell cycles from the early stages of SWCNT-cell interaction after cell attachment

to the substrate till the late stage of 80% cellular confluence before the reseeding procedure. It shows that within the first hour of cell cultivation with SWCNT-DNA complexes at a final concentration of 5 μm/mL, endocytosis of the complexes and gradual accumulation of SWCNT-DNA agglomerates in the cell cytoplasm occurs. Subsequently, the number of intracellular agglomerates and their size (up to 2 μm in diameter) increase, leading to an increase of the intensity of the G-band in SWCNT Raman spectra. During the whole period of cell growth in the presence of SWCNT-DNA complexes, SWCNTs do not penetrate the cell nuclei, and agglomerates are formed only in the cytoplasm. The Raman spectra of SWCNT agglomerates inside the cytoplasm indicate a time-dependent increase in the SWCNT content inside the cell (see Figure 2f-2o). However, the Raman spectrum contains not only D, G and 2D bands of SWCNTs, but also a wide band 2800-3000 cm^{-1} comprising vibration modes of the lipids' hydrocarbon chains at 2850 cm^{-1} (νCH_2 symmetrical mode), 2890 cm^{-1} (νCH_2 asymmetrical mode) and 2935 cm^{-1} (νCH_3 vibration) [26]. The presence of these bands is a signature of a lipid shell around the agglomerate, i.e., a membrane of the transport vesicle or lysosome. Intracellular accumulation of the SWCNTs is also accompanied by the slight growth of the D/G ratio for up to 0.26 (see Figure 2k-2o). In Figure 2n, the D/G ratio was not performed because of the strong overlapping of lipids and SWCNT Raman spectra in the range 1200-1500 cm^{-1}.
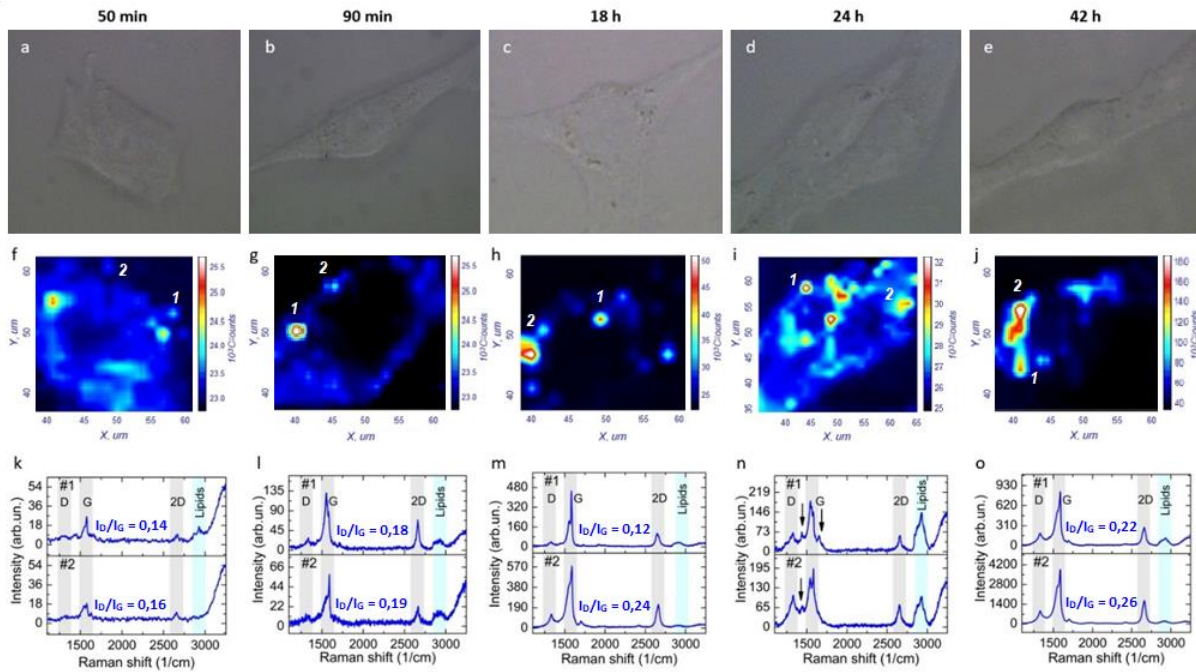
Figure 2. Distribution of SWCNT-DNA in the cell, 5 µg/mL, restored using the G-mode in the Raman spectrum of SWCNT: after (a, f) 50 min, (b, g) 90 min, (c, h) 18 h, (d, i) 24 h and (e, j) 42 h of cultivation in the presence of SWCNT-DNA complexes. The spectra of SWCNTs in (k-o) correspond to the agglomerates marked with the numbers in (f-j).

3.3 *Deferred SWCNT-DNA effects: cell proliferation over routine passaging*

To assess the effect of SWCNTs accumulated in cells on their proliferative ability and to evaluate the efficiency of removing SWCNTs from the cell cytoplasm, the cells exposed to SWCNT-DNA during the first passage were re-seeded until there were no SWCNTs left in the cytoplasm. SWCNTs in cells were visualized using Raman microscopy. During the first passage, the cells were exposed to SWCNT-DNA complexes at a concentration of 15 µg/mL, providing 50% cell survival. Survived and accumulated SWCNTs cells were used for further cultivation. During the following passages, SWCNT-DNA complexes were excluded from the extracellular environment.

It was established that prolonged cultivation of C6 cells (8-10 passages) in the presence of SWCNT-DNA complexes caused a decrease in the number of viable cells over 1-4 passages, in comparison with control cells without complexes and control cells cultivated in the presence of DNA. Thereafter, an intensification of cell proliferative activity during the 5th passage in the

presence of SWCNTs occurred, followed by equalization of cell number in samples with and without SWCNTs afterwards (see Figure 3a).

Interestingly, the replacement of double-stranded DNA in the SWCNT-DNA complex by short single-stranded oligonucleotides (ON) also led to the accumulation of SWCNTs inside the cells (see Supporting Information Figure S4). However, the agglomerates were significantly smaller than for the case of SWCNT-DNA complexes, and SWCNT-ON accumulation took a significantly longer time than that for SWCNT-DNA complexes (72h vs. 18h, see Supporting Information Figure S1). The number of viable cells in samples exposed to SWCNT-ON complexes was higher than that exposed to SWCNT-DNA ones. At the same time, almost complete removal of SWCNT-ON from cells occurred already after the 3rd passage. Nevertheless, the phenomenon of stimulating cell proliferation during the removal of SWCNTs persisted (Figure 3b, 4th passage).
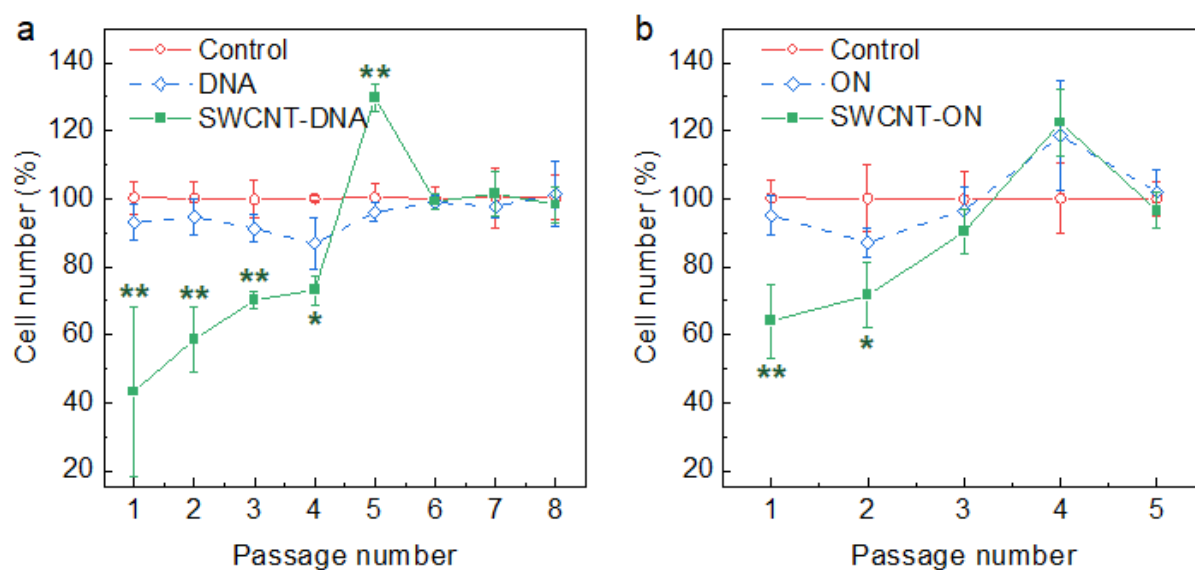
Figure 3. Modification of C6 cells proliferative activity during prolonged cultivation of cells exposed to SWCNT-DNA (a) and SWCNT-ON (b) complexes. Concentrations of SWCNT-DNA and SWCNT-ON in the culture medium is 15 μg/mL during the 1st passage. There were no SWCNT-DNA or SWCNT-ON in the medium on subsequent passages. The lines connecting the symbols in the graphs are shown only for convenience to indicate the trend. Data are mean ± SD values of duplicates from three independent experiments. *$p < 0.05$, **$p < 0.01$ refer to both control and DNA (or ON).

It is important to note that a long period of the SWCNT-ON accumulation may complicate their practical applications because SWCNTs elimination from the organism will start before the tumor accumulates SWCNTs. Thus, SWCNT-ON complexes would be more likely accumulated in liver cells or already secreted from the organism [27].

Moreover, previously we showed that the size and shape of the SWCNT agglomerates on a par with their photophysical properties play a crucial role in the effectiveness of the cold photothermoacoustic destruction of cells. Individual SWCNT-DNA or their bundles outside the cell are inactive in photothermoacoustics, but irradiation of one-micron-sized agglomerates of SWCNT-DNA inside the cell with pico-second NIR pulses leads to the photothermoacoustic destruction of the cell [16]. On the other hand, irradiation of agglomerates of smaller sizes (<0.5 μm diameter) cannot produce photoacoustic waves of sufficient magnitude to destruct the membrane (<<0.7 MPa). In comparison, when agglomerates are as big as 3 μm, the generated photoacoustic waves may exceed 4.5 MPa (see Supporting Information Figure S5). From this point of view, SWCNT-ON complexes do not meet the theranostic requirements because the small size of the agglomerates makes photothermoacoustic destruction of tumor cells difficult and increases accumulation time.

3.4 *Rapid and postponed mitochondrial response to SWCNT-DNA accumulation*

The functional metabolic status of mitochondria can be described in terms of the mitochondrial membrane potential ($\Delta\psi_{mit}$) and reactive oxygen species (ROS) production changes [28]. Figure 4a summarizes the data we obtained from the averaged fluorescence spectra of JC-1 in C6 glioma cells. The ratio of the fluorescence intensities of JC-1 at wavelengths of 590 nm and 530 nm (I_{fl590} / I_{fl530}), which characterizes the relative change in $\Delta\psi_{mit}$, undergoes considerable changes during the cultivation of C6 glioma cells exposed to SWCNT-DNA complexes. During the first 3 h of the cell interaction with SWCNTs, we registered an increase in the $\Delta\psi_{mit}$, while after 11 h of the exposure of glioma cells to SWCNT-DNA complexes, a decrease in $\Delta\psi_{mit}$ to the level of the control cells was observed (see Figure 4a). In contrast, when C6 glioma cells

were exposed to pure DNA at the same concentration, no significant changes in the mitochondrial potential were detected. This finding indicates that the observed effect is not associated with the DNA molecule.
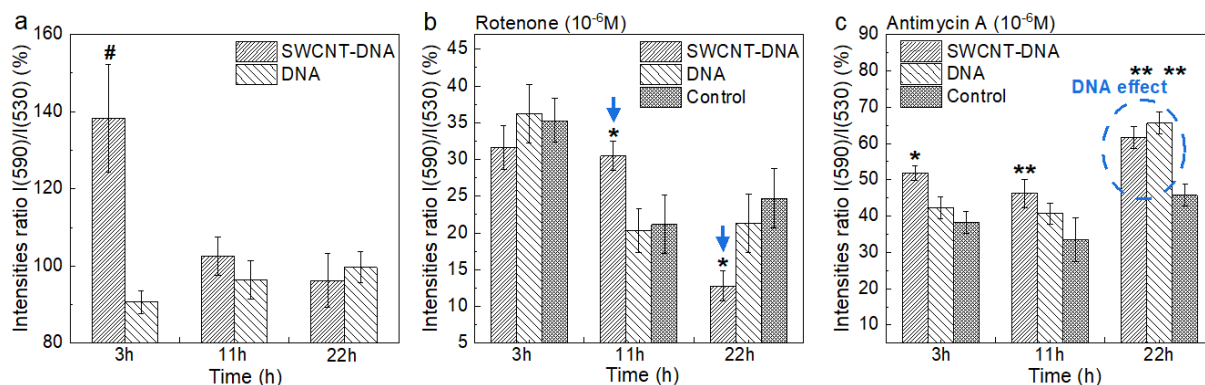
Figure 4. Mitochondrial membrane potential of C6 glioma cells in the presence of SWCNT-DNA. a – cells without electron-transport chain inhibitors, b – cells pretreated with 1 µM rotenone, c – cells pretreated with 1 µM antimycin A. Inhibitors were added 5 min before the mitochondrial potential measurement. Data are presented in % of the value of the cell $\Delta\psi_{mit}$ in the absence of inhibitors. The value of the $\Delta\psi_{mit}$ in control is taken equal to 100%. Data are mean ± SD values of duplicates from three independent experiments. #p < 0.001 refers to DNA samples, *p < 0.01 refers to both DNA and Control samples, **p < 0.05 refers to Control.

One of the consequences of high mitochondrial membrane potential is an increase in adenosine triphosphate (ATP) production [29]. ATP molecules are responsible for storing and transferring energy in living cells [30]. The main by-product of oxidative phosphorylation (ATP synthesis) is the superoxide anion, produced via a leak of electrons from the mitochondrial respiratory chain to O_2 [31]. As mitochondria are considered as one of the main sources of ROS in the cell, strengthening/weakening ROS production may significantly impact the intracellular signaling and regulation of cellular functioning.

We revealed that experimentally detected increase in $\Delta\psi_{mit}$ upon accumulation of SWCNT-DNA by cells was strongly correlated with the level of the superoxide anion radicals produced by mitochondria. As shown in Figure 5a, in 3h after the SWCNT-DNA addition to C6 cells, a 2-fold increase in the concentration of the superoxide anion radical was recorded. Further exposure of cells to SWCNT-DNA complexes (11 h and 22 h) led to a slight decrease

in the superoxide anion radical level compared to the control cells or cells exposed to DNA (see Figure 5a).

To reveal the mechanism of regulation of mitochondrial functions during the interaction of cells with SWCNTs, $\Delta\psi_{mit}$ and ROS production analysis using inhibitors of the mitochondrial electron transport chain (ETC) – rotenone and antimycin A – were performed. Rotenone inhibits the transfer of an electron from the iron-sulfur cluster in complex I to ubiquinone in the mitochondrial ETC. Since complex I cannot transfer electrons to ubiquinone, there is an excess of electrons in the form of NADH in the mitochondrial matrix. As a result, oxygen is reduced to ROS [32]. Antimycin A binds to the Q_{in} center of cytochrome bc_1 in complex III and inhibits the reduction of ubiquinone [33]. Resultantly, the cycle in which the enzyme works is interrupted. The cytochrome bc_1 complex is the central enzyme in the mitochondrial ETC and contributes to oxidative phosphorylation. Therefore, inhibition of this complex drastically reduces the formation of an electrochemical gradient on the inner mitochondrial membrane. As a result, there is a decrease in ATP production since ATP synthase lacks protons [34], [35]. In addition, inhibition of the complex III enhances the formation of superoxide anion radicals and other ROS [36], [37].

Inhibition of the mitochondrial ETC with 1 μM of rotenone causes a 65-70% decrease in $\Delta\psi_{mit}$ for cells exposed to SWCNT-DNA complexes for 3h, as compared to the control cells without the inhibitor, as presented in Figure 4b. Rotenone-induced decrease in the $\Delta\psi_{mit}$ was affected neither by SWCNT-DNA nor by DNA. This indicates that during the initial phase of SWCNT-DNA accumulation, the inhibition of the electron transfer in the ETC by rotenone does not change.

A significant difference in the rotenone-induced decrease in the $\Delta\psi_{mit}$ is observed in C6 cells exposed to SWCNT-DNA compared to DNA and control cells after 11 h of cultivation (Figure 4b). Specifically, the value of $\Delta\psi_{mit}$ is decreased for cells exposed to SWCNT-DNA, but it was approx. 1.5 times higher than that for cells exposed to DNA and control cells under

18

the rotenone action. The opposite situation is observed after 22 h of cell exposure to SWCNT-DNA, DNA, and control cells. In the presence of SWCNT-DNA complexes, almost complete depolarization (13% of the control) of the inner mitochondrial membrane is detected, although partial depolarization (approx. 25% of control w/o rotenone) is observed for cells exposed to DNA or control cells. In all cases, there is no significant difference in $\Delta\psi_{mit}$ depolarization in the presence of DNA and control cells, confirming the involvement of the SWCNTs in the electron transfer process in complex I of the ETC.

At the early stage of SWCNT accumulation during endocytosis, the interaction of SWCNT-DNA complexes occurs mainly with the cell membrane structures but not with intracellular organelles. And the significant hyperpolarization of the mitochondrial membrane is associated with increased ATP production for additional cell energy supply (Figure 4a). This effect is vanished by rotenone in 3h of cell-nanoparticle interaction (Figure 4b). Accumulation of SWCNTs inside the cell differently influences the electron transfer in rotenone-effected cells depending on the SWCNTs accumulation time. Specifically, the SWCNTs accumulation for 11h and 22h reduces and enhances the depolarizing effect of rotenone, respectively, indicating the change in the energy supply mechanisms in cells and the involvement of electron transfer in complex I.

Antimycin A inhibition of the electron transfer in the ETC of mitochondria leads to the transmembrane potential decrease (Figure 4c). During the initial phase of SWCNT accumulation (after 3h) antimycin-induced depolarization is less than in cells exposed to DNA or in control cells, confirming the energy dependence of the SWCNT-DNA intracellular transport. The same trend is observed after 11h and 22h of cell exposure to SWCNT-DNA complexes. However, the influence of the DNA molecules in the restoration of the mitochondrial membrane potential prevails, as $\Delta\psi_{mit}$ is the same in the presence of only DNA molecules and SWCNT-DNA complexes compared to the control cells after 22 h (Figure 4c).

According to the data presented in Figure 5b, rotenone and antimycin led to an almost 90% decrease in ROS levels in cells not exposed to SWCNT-DNA or DNA compared to control cells without inhibitors. Cells' exposure to SWCNT-DNA resulted in an additional reduction in the ROS level in case of interruption of electron transfer in both complexes I and III. Nevertheless, these decreases are caused by different mechanisms. In the case of inhibition of the complex III by antimycin DNA is assumed to act as an interceptor of free radical products, as DNA molecules themselves caused an equivalent decrease in the ROS production as SWCNT-DNA complexes. Nevertheless, ROS decrease evoked by SWCNT-DNA complexes in rotenone-pretreated cells was not associated with the interception of electrons by DNA molecules.
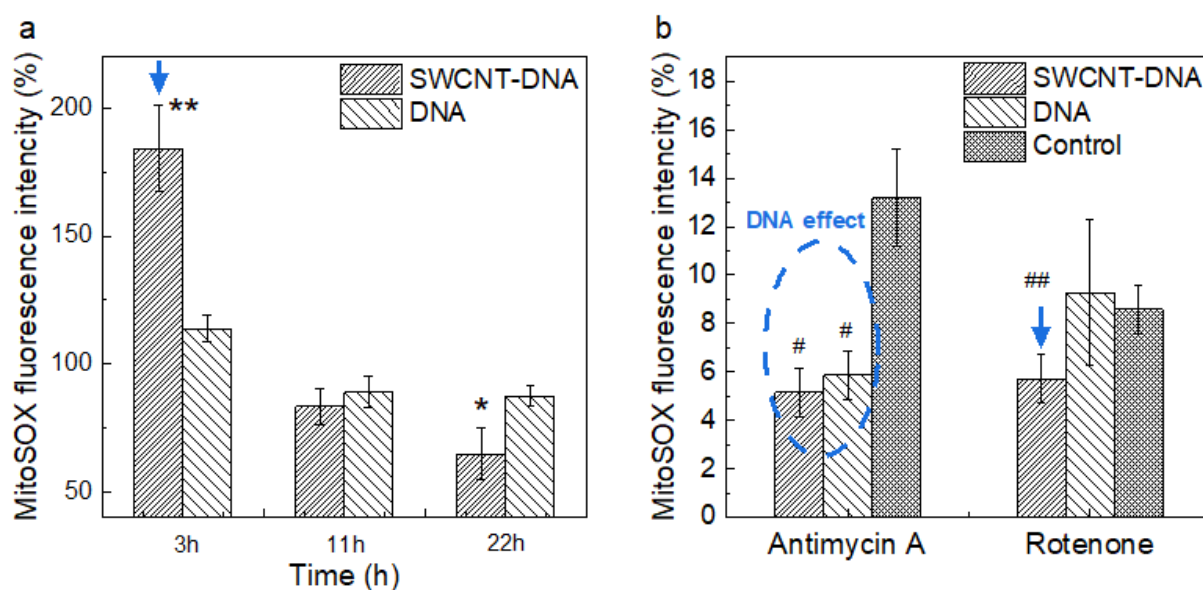
Figure 5. The level of superoxide anion radical production by mitochondria in rat C6 glioma cells after DNA or SWCNT-DNA administration: a – over-time changes in mitochondria ROS production without inhibitor addition, b – level of superoxide anion radical production upon rotenone and antimycin addition after 11 h in control cells, and after DNA or SWCNT-DNA administration. Inhibitors were added 5 min before the measurement of the superoxide anion radical level. The final concentration of rotenone and antimycin in cell culture was 1 μM. Measurements were performed using MitoSOx Red. Data are mean ± SD values of duplicates from three independent experiments. *$p < 0.05$, **$p < 0.01$ refer to DNA samples. #$p < 0.01$, ##$p < 0.05$ refers to Control.

Fluorescence microscopy with JC-1 dye enables visualization of the distribution of mitochondria inside the cell and pointing out the mitochondria with high membrane potential

[38]. Figure 4a demonstrates that cell cultivation in the presence of SWCNT-DNA over 22 h induced no significant mitochondrial membrane potential change. However, as shown in Figure 6 the distribution of mitochondria changed after SWCNT accumulation inside the cell. The formation of empty space without mitochondria in the cytoplasm in the area where nanotubes are located, and a 'ring' of mitochondria around the SWCNTs (see regions marked with arrows in Figure 6a) indicates that SWCNTs are assembled into agglomerates inside the cytoplasm, but they are unevenly distributed between intracellular organelles. Moreover, since the JC-1 fluorescence at $\lambda_{em} = 590$ nm (Figure 6b, marked with arrows) is stronger than that at $\lambda_{em} = 530$ nm evidence (see Figure 6a), the highly energized mitochondria surround SWCNT agglomerates. Nevertheless, visualization of mitochondria with JC-1 allows us to conclude that SWCNTs do not penetrate into the cell nucleus (Figure 6c); however, agglomerated SWCNTs deform the nucleus' membranes.
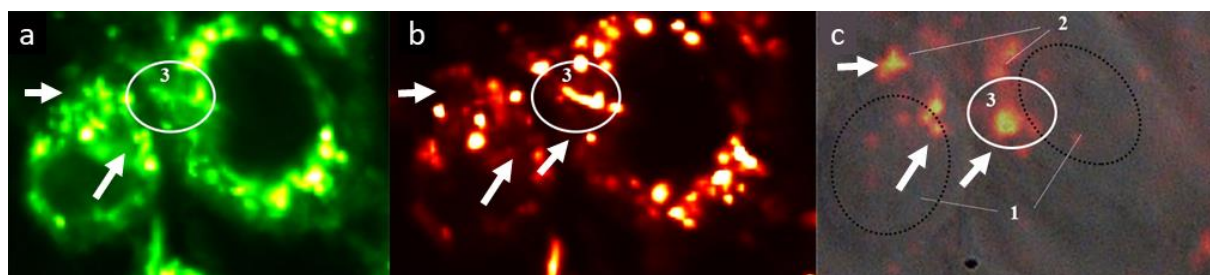

Figure 6. Typical images of mitochondria distribution in rat C6 glioma cells (after 22 h of cultivation in the presence of SWCNT-DNA complexes). a – JC-1 fluorescence at $\lambda_{em} = 530$ nm, b – JC-1 fluorescence at $\lambda_{em} = 590$ nm, c – SWCNT-DNA complexes distribution. 1 – Cell nuclei, 2 – SWCNT-DNA complexes, 3 – localization of SWCNT-DNA complexes and functionally active mitochondria with high mitochondrial membrane potential $\Delta\psi_{mit}$. Arrows mark the localization of SWCNT-DNA agglomerates.

Phenomena observed indicates the shift in the cellular redox state during the accumulation of SWCNT-DNA complexes, which still demands further specific targeted investigation of total ROS generation and modification of antioxidant status. The focus of our future studies will be mechanisms of redox regulation throughout all steps of the interaction of SWCNT and living cells.

4. Conclusion

We performed a systemic study of the interaction of the SWCNT-DNA complex with glioma cells starting from the SWCNT interaction with the cell membrane till complete removing SWCNTs from the cell cytoplasm. We also demonstrate the viability of cells containing SWCNTs in the cytoplasm and their ability to maintain the life cycle over several passages.

The accumulation dynamics, intracellular distribution and localization make SWCNT-DNA complexes the most appropriate candidate for biomedical applications because they meet all the requirements for cold photothermoacoustics. Moreover, SWCNT-DNA complexes are shown to be accumulated fast inside the cell cytoplasm via micropinocytosis leading to F-actin reorganization and quick mitochondria hyperpolarization and ROS production due to energy consumption during endocytosis, with further normalization of mitochondrial function after the saturation of SWCNT concentration in the cytoplasm. The spreading of SWCNTs inside C6 glioma cells is fast; SWCNTs localize as micron-sized agglomerates surrounded by actively functioning mitochondria causing their shape modification. Further cultivation of cells with accumulated SWCNTs shows that SWCNTs are biochemically inert for the cells, that is expressed in the absence of any changes in the functioning of cell mitochondria after reaching the maximal concentration of SWCNTs in the cytoplasm, as well as in the restoration of the cell population, after several passages resulting in complete removal of SWCNTs from cells (data summarized in Figure 7).
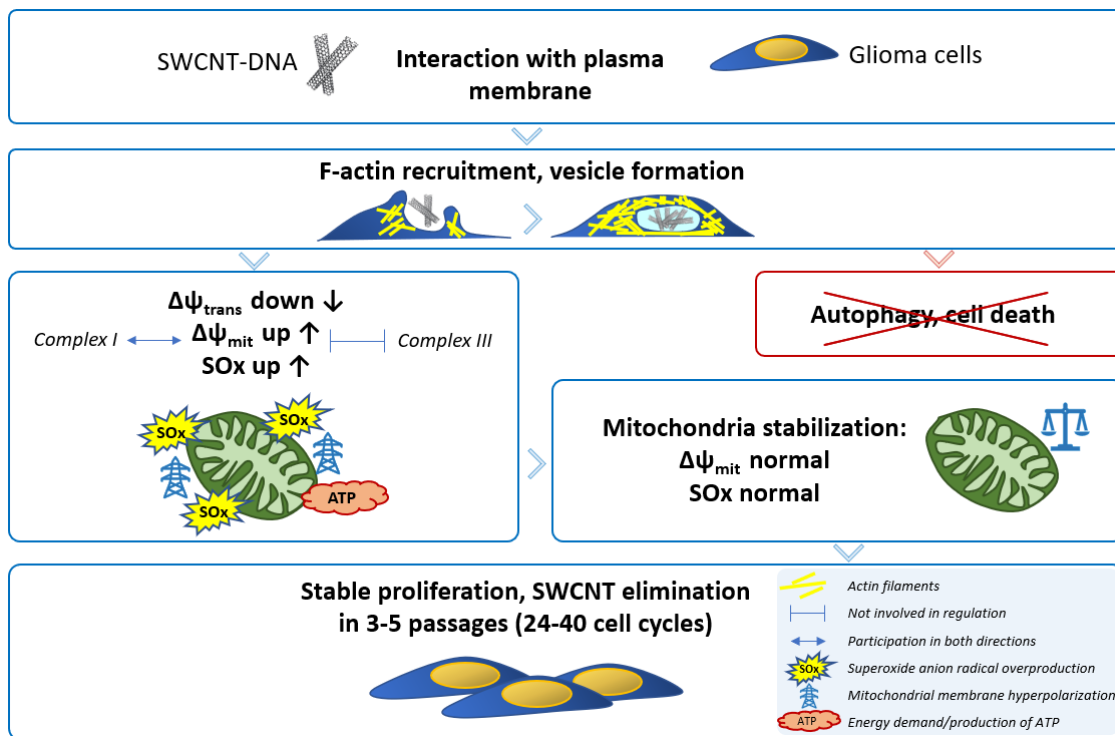
Figure 7. Scheme of SWCNT-DNA quick and postponed effects on C6 glioma cell functions during cell interaction with SWCNTs

The combination of appropriate physicochemical properties of SWCNTs (high absorption in NIR, good dispersion of the environment outside the cell and agglomeration of SWCNTs inside the cell, intense Raman spectrum) together with their relative biological inertness and the ability to rapidly accumulate in and slowly excrete from tumor cells allows the development of a wide range of cancer treatment methods and theranostics approaches with the emphasis on safety, personalization and enhanced therapeutic efficacy.

References

[1]   H. Chen, W. Zhang, G. Zhu, J. Xie, X. Chen, Rethinking cancer nanotheranostics, Nat. Rev. Mater. 2 (2017). https://doi.org/10.1038/natrevmats.2017.24.

[2]   Z. Yang, Z. Sun, Y. Ren, X. Chen, W. Zhang, X. Zhu, Z. Mao, J. Shen, S. Nie, Advances in nanomaterials for use in photothermal and photodynamic therapeutics (Review), Mol. Med. Rep. 20 (2019) 5–15. https://doi.org/10.3892/mmr.2019.10218.

[3]   L. Li, J. Li, Y. Shi, P. Du, Z. Zhang, T. Liu, R. Zhang, Z. Liu, On-Demand Biodegradable Boron Nitride Nanoparticles for Treating Triple Negative Breast Cancer with Boron Neutron Capture Therapy, ACS Nano. 13 (2019) 13843–13852. https://doi.org/10.1021/acsnano.9b04303.

[4]   N. Anzar, R. Hasan, M. Tyagi, N. Yadav, J. Narang, Carbon nanotube - A review on Synthesis, Properties and plethora of applications in the field of biomedical science, Sensors Int. 1 (2020) 100003. https://doi.org/10.1016/j.sintl.2020.100003.

[5]   A. Eatemadi, H. Daraee, H. Karimkhanloo, M. Kouhi, N. Zarghami, A. Akbarzadeh, M. Abasi, Y. Hanifehpour, S.W. Joo, Carbon nanotubes: Properties, synthesis, purification, and medical applications, Nanoscale Res. Lett. 9 (2014) 1–13. https://doi.org/10.1186/1556-276X-9-393.

[6]   N. Saifuddin, A.Z. Raziah, A.R. Junizah, Carbon nanotubes: A review on structure and their interaction with proteins, J. Chem. (2013). https://doi.org/10.1155/2013/676815.

[7]   H. Zare, S. Ahmadi, A. Ghasemi, M. Ghanbari, N. Rabiee, M. Bagherzadeh, M. Karimi, T.J. Webster, M.R. Hamblin, E. Mostafavi, Carbon nanotubes: Smart drug/gene delivery carriers, Int. J. Nanomedicine. 16 (2021) 1681–1706. https://doi.org/10.2147/IJN.S299448.

[8]   W. Zhang, Z. Zhang, Y. Zhang, The application of carbon nanotubes in target drug delivery systems for cancer therapies, Nanoscale Res. Lett. 6 (2011) 1–22. https://doi.org/10.1186/1556-276X-6-555.

[9]   E.N. Golubewa, M.V. Shuba, M.V. Vasilieu, T.A. Kulahava, Application of Raman Spectroscopy for Analysis of Carbon Nanotube Distribution in Living Cells, J. Appl. Spectrosc. 85 (2019). https://doi.org/10.1007/s10812-019-00768-7.

[10]   C. Fang, M. Zhang, Nanoparticle-based theragnostics: Integrating diagnostic and therapeutic potentials in nanomedicine, J. Control. Release. 146 (2010) 2–5. https://doi.org/10.1016/j.jconrel.2010.05.013.

[11]   P.C. Ma, N.A. Siddiqui, G. Marom, J.K. Kim, Dispersion and functionalization of carbon nanotubes for polymer-based nanocomposites: A review, Compos. Part A Appl. Sci. Manuf. 41 (2010) 1345–1367. https://doi.org/10.1016/j.compositesa.2010.07.003.

[12]   L.N. Golubewa, T.A. Kulahava, Y.S. Leonik, M. V. Shuba, G.N. Semenkova, Application of Raman Spectroscopy for Studying the Mechanisms of Neutrophil Activation by Carbon Nanotubes, J. Appl. Spectrosc. 88 (2021) 77–84. https://doi.org/10.1007/s10812-021-01143-1.

[13]   K. Donaldson, R. Aitken, L. Tran, V. Stone, R. Duffin, G. Forrest, A. Alexander, Carbon nanotubes: A review of their properties in relation to pulmonary toxicology and workplace safety, Toxicol. Sci. 92 (2006) 5–22. https://doi.org/10.1093/toxsci/kfj130.

[14]   J. Semberova, S.H. De Paoli Lacerda, O. Simakova, K. Holada, M.P. Gelderman, J. Simak, Carbon nanotubes activate blood platelets by inducing extracellular Ca 2+ influx sensitive to calcium entry inhibitors, Nano Lett. 9 (2009) 3312–3317. https://doi.org/10.1021/nl901603k.

[15]   M. Roldo, D.G. Fatouros, Biomedical applications of carbon nanotubes, Annu. Reports Prog. Chem. - Sect. C. 109 (2013) 10–35. https://doi.org/10.1039/c3pc90010j.

[16]   L. Golubewa, I. Timoshchenko, O. Romanov, R. Karpicz, T. Kulahava, D. Rutkauskas, M. Shuba, A. Dementjev, Y. Svirko, P. Kuzhir, Single-walled carbon nanotubes as a photo-thermo-acoustic cancer theranostic agent: theory and proof of the concept experiment, Sci. Rep. 10 (2020). https://doi.org/10.1038/s41598-020-79238-6.

[17]   M. V. Shuba, A.G. Paddubskaya, P.P. Kuzhir, S.A. Maksimenko, V.K. Ksenevich, G. Niaura, D. Seliuta, I. Kasalynas, G. Valusis, Soft cutting of single-wall carbon nanotubes by low temperature ultrasonication in a mixture of sulfuric and nitric acids, Nanotechnology. 23 (2012) 9. https://doi.org/10.1088/0957-4484/23/49/495714.

[18]   X. Cui, B. Wan, Y. Yang, X. Ren, L.H. Guo, Length effects on the dynamic process of cellular uptake and exocytosis of single-walled carbon nanotubes in murine macrophage cells /631/80 /704/172 /82/29 /14/19 /14/34 /123 article, Sci. Rep. 7 (2017) 1–13. https://doi.org/10.1038/s41598-017-01746-9.

[19]   I.A. Chelnokova, L.N. Golubewa, M.N. Starodubtseva, T.A. Kulahava, Y.N. Kunitskaya, P.M. Bulai, I.E. Starodubtsev, Y.S. Kharin, M. V. Shuba, Effect of single-walled carbon nanotubes on the structural, physical and mechanical properties of rat glial cell surface, J. Nanoparticle Res. 22 (2020) 144. https://doi.org/10.1007/s11051-020-04856-0.

[20]   H.L. Liu, Y.L. Zhang, N. Yang, Y.X. Zhang, X.Q. Liu, C.G. Li, Y. Zhao, Y.G. Wang, G.G. Zhang, P. Yang, F. Guo, Y. Sun, C.Y. Jiang, A functionalized single-walled carbon nanotubeinduced autophagic cell death in human lung cells through Akt-TSC2-mTOR signaling, Cell Death Dis. 2 (2011) e159. https://doi.org/10.1038/cddis.2011.27.

[21]   M. Ghosh, S. Murugadoss, L. Janssen, S. Cokic, C. Mathyssen, K. Van Landuyt, W. Janssens, S. Carpentier, L. Godderis, P. Hoet, Distinct autophagy-apoptosis related pathways activated by Multi-walled (NM 400) and Single-walled carbon nanotubes (NIST-SRM2483) in human bronchial epithelial (16HBE14o-) cells, J. Hazard. Mater. 387 (2020). https://doi.org/10.1016/j.jhazmat.2019.121691.

[22]   E.J. Park, N.E.M. Zahari, E.W. Lee, J. Song, J.H. Lee, M.H. Cho, J.H. Kim, SWCNTs induced autophagic cell death in human bronchial epithelial cells, Toxicol. Vitr. 28 (2014) 442–450. https://doi.org/10.1016/j.tiv.2013.12.012.

[23]   H. Morishita, N. Mizushima, Diverse cellular roles of autophagy, Annu. Rev. Cell Dev. Biol. 35 (2019) 453–475. https://doi.org/10.1146/annurev-cellbio-100818-125300.

[24]   L. Shang, S. Chen, F. Du, S. Li, L. Zhao, X. Wang, Nutrient starvation elicits an acute autophagic response mediated by Ulk1 dephosphorylation and its subsequent dissociation from AMPK, Proc. Natl. Acad. Sci. U. S. A. 108 (2011) 4788–4793. https://doi.org/10.1073/pnas.1100844108.

[25]   A. Niemann, A. Takatsuki, H.P. Elsässer, The lysosomotropic agent monodansylcadaverine also acts as a solvent polarity probe, J. Histochem. Cytochem. 48 (2000) 251–258. https://doi.org/10.1177/002215540004800210.

[26]   D.W. Shipp, F. Sinjab, I. Notingher, Raman spectroscopy: techniques and applications in the life sciences, Adv. Opt. Photonics. 9 (2017) 315. https://doi.org/10.1364/aop.9.000315.

[27]   W. Poon, Y.N. Zhang, B. Ouyang, B.R. Kingston, J.L.Y. Wu, S. Wilhelm, W.C.W. Chan, Elimination Pathways of Nanoparticles, ACS Nano. 13 (2019) 5785–5798. https://doi.org/10.1021/acsnano.9b01383.

[28]   J.M. Suski, M. Lebiedzinska, M. Bonora, P. Pinton, J. Duszynski, M.R. Wieckowski, Relation between mitochondrial membrane potential and ROS formation, Methods Mol. Biol. 810 (2012) 183–205. https://doi.org/10.1007/978-1-61779-382-0_12.

[29]   L.D. Zorova, V.A. Popkov, E.Y. Plotnikov, D.N. Silachev, I.B. Pevzner, S.S. Jankauskas, V.A. Babenko, S.D. Zorov, A. V. Balakireva, M. Juhaszova, S.J. Sollott, D.B. Zorov, Mitochondrial membrane potential, Anal. Biochem. 552 (2018) 50–59. https://doi.org/10.1016/j.ab.2017.07.009.

[30]   P. Neupane, S. Bhuju, N. Thapa, H.K. Bhattarai, ATP Synthase: Structure, Function and Inhibition, Biomol. Concepts. 10 (2019) 1–10. https://doi.org/10.1515/bmc-2019-0001.

[31]   M.P. Murphy, How mitochondria produce reactive oxygen species, Biochem. J. 417 (2009) 1–13. https://doi.org/10.1042/BJ20081386.

[32]   R.Z. Zhao, S. Jiang, L. Zhang, Z. Bin Yu, Mitochondrial electron transport chain, ROS generation and uncoupling (Review), Int. J. Mol. Med. 44 (2019) 3–15.

https://doi.org/10.3892/ijmm.2019.4188.

[33] L.S. Huang, D. Cobessi, E.Y. Tung, E.A. Berry, Binding of the respiratory chain inhibitor antimycin to the mitochondrial bc1 complex: A new crystal structure reveals an altered intramolecular hydrogen-bonding pattern, J. Mol. Biol. 351 (2005) 573–597. https://doi.org/10.1016/j.jmb.2005.05.053.

[34] J.P. Mazat, S. Ransac, The cytochrome bc1 complex in the mitochondrial respiratory chain functions according to the Q cycle hypothesis of Mitchell: The proof using a stochastic approach?, Medecine/Sciences. 26 (2010) 1079–1086. https://doi.org/10.1051/medsci/201026121079.

[35] M. Saraste, Oxidative phosphorylation at the fin de siecle, Science (80-.). 283 (1999) 1488–1493. https://doi.org/10.1126/science.283.5407.1488.

[36] L. Bleier, S. Dröse, Superoxide generation by complex III: From mechanistic rationales to functional consequences, Biochim. Biophys. Acta - Bioenerg. 1827 (2013) 1320–1331. https://doi.org/10.1016/j.bbabio.2012.12.002.

[37] J.F. Turrens, Mitochondrial formation of reactive oxygen species, J. Physiol. 552 (2003) 335–344. https://doi.org/10.1113/jphysiol.2003.049478.

[38] F. Sivandzade, A. Bhalerao, L. Cucullo, Analysis of the Mitochondrial Membrane Potential Using the Cationic JC-1 Dye as a Sensitive Fluorescent Probe, Bio-Protocol. 9 (2019). https://doi.org/10.21769/bioprotoc.3128.